JACS
JOURNAL OF THE AMERICAN CHEMICAL SOCIETY
pubs.acs.org/JACS
Communication

Multipolar Raman Scattering vs Interfacial Nanochemistry: Case of 4-Mercaptopyridine on Gold

Alexander B. C. Mantilla, Chih-Feng Wang, Yi Gu, Zachary D. Schultz, and Patrick Z. El-Khoury*

Cite This: J. Am. Chem. Soc. 2022, 144, 20561−20565
Read Online
ACCESS | Metrics & More | Article Recommendations | Supporting Information

ABSTRACT: Caution needs to be exercised in associating changes in plasmon-enhanced Raman spectra with chemical transformations. This is demonstrated through a detailed analysis of tip-enhanced Raman (TER) scattering from 4-mercaptopyridine (MPY) on gold. The substrate used consists of gold nanoplates atop a gold surface featuring heterogeneous grooves, all coated with a monolayer of MPY. The brightest spectra across the substrate exhibit features that can only be recovered by considering the generalized polarizability of oriented MPY molecules. The complex TER spectra we observe do not mark interfacial chemistry but rather multipolar TER scattering driven by local field gradients.

Several physical and chemical phenomena may lead to plasmon-enhanced molecular Raman spectra that differ significantly from their conventional ensemble-averaged analogues.[1] These effects have been discussed in several studies that utilized tip-enhanced Raman (TER) spectral imaging and related techniques to visualize and identify molecules at various interfaces with high spatial resolution and sensitivity.[2] In the absence of electronic resonances of pure molecular or mixed metal-molecule origin, the first thing to consider would be surface selection rules.[3,4] In TER spectroscopy and imaging, the subject of this report, the local field is typically enhanced in the direction parallel to the scanning probe tip.[5] This leads to molecular-orientation-dependent TER spectra, both in the case of ultrasensitive/single-molecule measurements and for oriented molecular ensembles, such as the case of self-assembled monolayers. Besides modified relative intensities, non-resonant TER spectra often contain additional peaks that cannot be assigned based on standard Raman selection rules.[4,6] These additional modes may or may not belong to the subset of vibrational states of the molecules being probed. If they do not, the modified spectral patterns can sometimes be reliably associated with products of plasmon-induced/enhanced molecular charging and transformations.[7,8] We emphasize that spectral patterns, as opposed to the (dis)appearance of single peaks, need to be fully accounted for to convincingly substantiate the claim that a chemical transformation took place in the TER geometry.

In the absence of (electronic) resonance enhancement, sets of peaks arising from Raman forbidden transitions that do belong to the subset of vibrational states of the system often appear in TER spectra.[3,9,10] Such spectral patterns have been associated with multipolar Raman scattering driven by spatiotemporal local optical field gradients.[10,11] In prior measurements that targeted molecules that are structurally related to 4-mercaptopyridine (MPY), the subject of this report, tip-enhanced multipolar Raman scattering has been observed and assigned.[10] Multipolar Raman scattering has also been more generally observed in molecular surface-enhanced Raman scattering from plasmonic nanojunctions[4] and even in isolated molecules interrogated under the stability afforded by ultrahigh-vacuum and ultralow-temperature TER setups.[12] Yet, multipolar Raman scattering continues to be under-appreciated, even in the context of tracking chemical transformations using plasmon-enhanced Raman scattering.[11] This is surprising, given the prevalence of spectral fluctuations in high spatial resolution/ultrasensitive TER measurements, particularly under ambient conditions.[4,9,13] In this work, we stress the importance of considering multipolar Raman scattering to understand the brightest TER spectra of 4-MPY on gold.

The general topographic features of the substrate can be visualized using topographic atomic force microscopy (AFM) imaging, as shown in Figure 1a. The substrate consists of a relatively smooth (∼1 nm average roughness) polycrystalline gold substrate that features heterogeneous grooves. Single-crystal gold nanoplatelets were deposited on the gold surface, and a monolayer of MPY was self-assembled on the resulting substrate. The TER image (Figure 1b) of the dashed rectangular area that is highlighted in Figure 1a and its corresponding simultaneously recorded AFM image (Figure 1c) reveal that the edges of the nanosized grooves sustain the highest local optical field enhancement factors. This is consistent with a recent study from our group that analyzed the chemical images of similar, albeit smaller nanostructures that we patterned into gold using pulsed force nanolithography.[14] Higher spatial resolution correlated chemical (Figure 1d) and topographic (Figure 1e) images of an isolated nanogroove allow us to infer a spatial resolution on the order of ∼5 nm in TER imaging. Note that our measured spatial

Received: September 22, 2022
Published: November 7, 2022

https://doi.org/10.1021/jacs.2c10132
J. Am. Chem. Soc. 2022, 144, 20561−20565

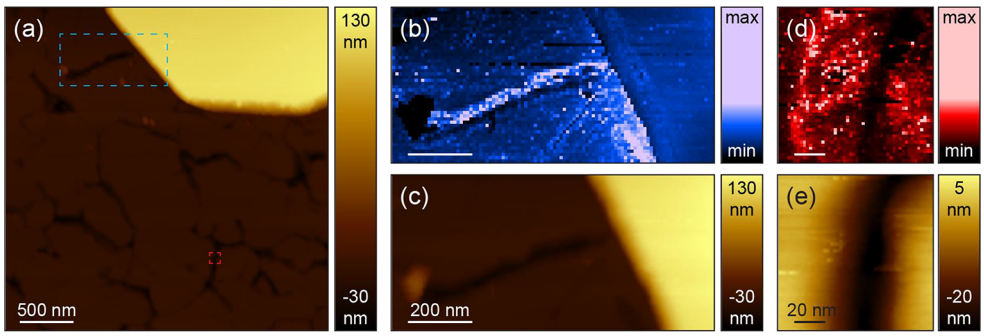

Figure 1. (a) Topographic AFM image of the MPY-coated substrate. The rectangular blue and square-shaped red areas highlighted in (a) are further analyzed through TER (b, d) and AFM (c, e) mapping. The chemical and topographic images of each of the areas were simultaneously measured in panels b–e. The ~1605 cm^{-1} TER chemical images were recorded using 150 mW of laser power, time-integrated for 0.5 s, and the lateral step sizes used were 10 nm (b) and 2 nm (d).

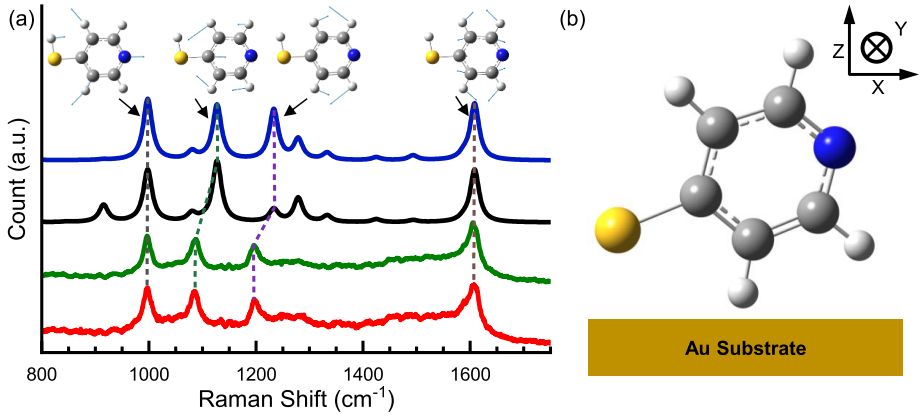

Figure 2. (a) Experimental and calculated non-resonant Raman spectra. Spatially averaged TER spectra across the entire field of view (red) vs atop the Au nanoplate (green) taken from Figure 1b are compared to orientationally averaged (black spectrum) vs orientation-specific (blue spectrum, see text for more details) theoretical spectra. The theoretical spectra were computed at the pbe0/tzvp level of theory, and the computed frequencies were linearly scaled by a single factor of 0.98. A vector representation of the normal modes is the upper part of (a). (b) Preferred molecular orientation that results in the blue spectrum in (a).

resolution is only limited by the gently varying local optical fields, and it may not reflect the actual spatial resolution of our measurements. We refrain from using pixel-to-pixel variations as a measure of spatial resolution because the signals are well known to fluctuate in time, even at a single tip position. We also note that the use of pixel-to-pixel variations as a gauge of spatial resolution is only appropriate when such variations are observed repeatedly in sequentially recorded TER scans.[15]

Spatial averaging of the TER spectra across the entire field of view shown in Figure 1b results in the red spectrum in Figure 2a. The spatiotemporally averaged spectrum is generally consistent with prior TER spectra of self-assembled monolayers of MPY.[16,17] It exhibits 4 predominant resonances at 1607, 1197, 1085, and 997 cm^{-1}. A vector representation of the displacements that lead to these resonances is shown toward the top of Figure 2a. The TER spectrum we obtain by spatial averaging of the optical response recorded exclusively on top of the gold nanoplate (green spectrum in Figure 2a) is very similar to the global average. This suggests the predominance of a single binding geometry of MPY across the substrate. The binding geometry can be established by considering TER selection rules. A numerically convenient approach to simulating the latter[5] involves scanning the field directions (indices *i,j,k*) in

$$S^2_{\mathrm{TERS}}\alpha \sum_n \left| \overrightarrow{E^{\mathrm{L}}_{\mathrm{s}}}(i,j,k)\, \widetilde{\alpha'_n}\, \overrightarrow{E^{\mathrm{L}}_{\mathrm{i}}}(i,j,k) \right|^2 \quad (1)$$

relative to a given (fixed) molecular orientation represented by its molecular polarizability derivative tensor elements $\widetilde{\alpha'_n}$. This results in a 10×10×10×*n* array, in which the first three indices (10×10×10) correspond to the three Cartesian axes/indices of $\overrightarrow{E^{\mathrm{L}}_{\mathrm{i,s}}}$ (normalized fields, scanned between 0.1 and 1 in increments of 0.1).[5] The fourth index (n = 30) denotes the vibrational modes of MPY. This is followed by recasting the tabulated point spectra as sums of normalized Lorentzian functions (width of 10 cm^{-1}) in the region of interest, which increases the dimensionality of the final index in the array to 951 to cover the 800–1750 cm^{-1} spectral range in 1 cm^{-1} increments. We then match the resulting spectral profiles to their experimental analogues using the sum of absolute differences (Manhattan distance) as a matching criterion.[5] After a successful match is obtained, we project the matched field direction to a commonly used laboratory frame (see Figure 2b). This naturally requires an identical rotation of the molecule using the same rotation matrix (and its inverse) to extract a molecular orientation relative to the preferred local optical field direction, namely along the tip axis (Z) that is orthogonal to the substrate plane (XY). Overall, eq 1 assumes a well-defined orientation of 4-MPY molecules with respect to

https://doi.org/10.1021/jacs.2c10132
J. Am. Chem. Soc. 2022, 144, 20561–20565

the local optical field that is predominantly enhanced along the tip axis. This is contrasted with orientationally averaged Raman scattering from molecular ensembles in conventional spectroscopic and microscopic measurements. The treatment is proper both for single molecules and for our present case of self-assembled monolayers.

Two calculated non-resonant Raman spectra are shown in Figure 2a. The black spectrum is the conventional orientationally averaged theoretical Raman spectrum. The computed frequency shifts agree with their experimental analogues for the 1607 and 997 cm^{-1} modes, whereas they are significantly overestimated in the case of the 1197 and 1085 cm^{-1} resonances. These somewhat expected differences arise from discrepancies between the isolated molecular model we consider *in silico* vs a self-assembled monolayer of interacting MPY molecules on gold. The computed relative intensities of the ensemble-averaged theoretical spectrum (black spectrum) also differ from their TER analogues. The correct relative intensity pattern can only be captured by considering the preferred molecular orientation following the above-described eq 1 and numerical approach. Indeed, the resulting blue spectrum in Figure 2a closely resembles its experimental analogues in terms of the relative intensities of the TER-active vibrational states. The match also allows us to infer the preferred molecular orientation across the substrate, which is schematically illustrated in Figure 2b.

We then zoom in and analyze the brightest 10% of the spectra across the region of interest that is visualized in Figure 1b,c. We found that roughly half of the spectra (only two of which are shown in Figure 3a,b) can be readily recovered by

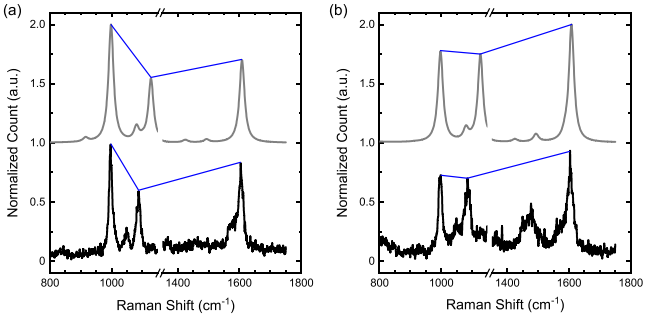

Figure 3. Single-pixel TER spectra (lower black traces in panels a and b) are compared to theoretical spectra (upper gray traces in panels a and b) computed following eq 1 in the text. Polarizability derivatives were computed at the pbe0/tzvp level of theory, and the computed frequencies were linearly scaled by a single factor of 0.98. Relative intensities are tracked using solid blues lines throughout.

considering distinct relative orientations of the MPY molecule relative to a unidirectional local electric field. Indeed, the representative spectra in Figure 3 show that the relative intensities of the TER-active vibrational states can be recovered following eq 1 and the matching protocol described above. Note that the results shown in Figure 3 (and below) do not take the 1197 cm^{-1} mode into account to facilitate spectral matching, since the corresponding computed peak position diverges the most from its experimental analogue.

Besides TER scattering that is sensitive to the orientation of the molecules relative to the local optical field, we also observed spectral patterns that cannot be recovered using eq 1 and conventional (dipolar) Raman selection rules more generally. Some of these spectra are collated in Figure 4 and

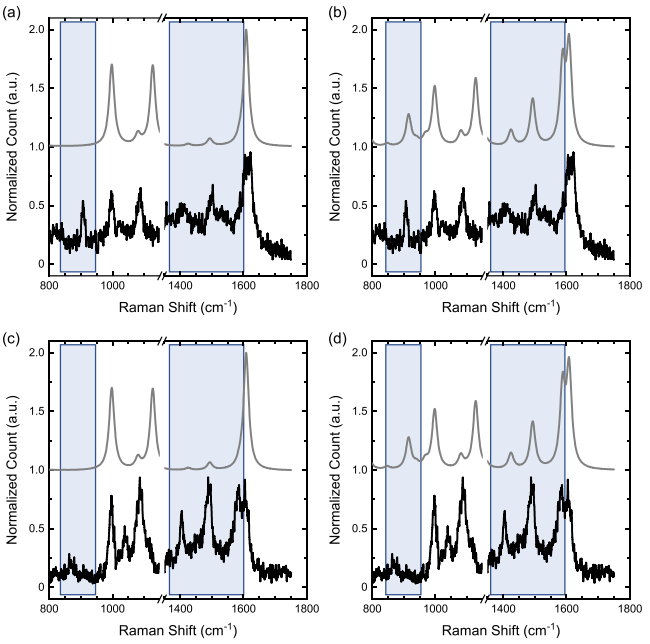

Figure 4. Single-pixel TER spectra taken near the grooves (lower black traces in all panels) are compared to theoretical spectra (upper gray traces in all panels). In the left panels a and c, only dipolar terms are considered (eq 1). In the right panels b and d, both dipolar and multipolar (only G'^2 here) terms are accounted for. All polarizability derivatives were computed at the pbe0/tzvp level of theory, and the computed frequencies were linearly scaled by a single factor of 0.98. The blue-shaded regions highlight peaks and spectral patterns that derive their intensities from multipolar TER scattering.

Figure S1 of the Supporting Information. In Figure 4a,c, we match two single-pixel TER spectra based on normal Raman selection rules, following eq 1. Much like the case described in Figure 3, we can recover the experimental relative intensities of the Raman-allowed peaks. The conventional analysis, however, misses several additional peaks that appear altogether. These peaks are highlighted using light blue rectangles in Figure 4. These spectral patterns can only be faithfully recovered by considering the generalized molecular polarizabilities of MPY:[18]

$$\alpha_{\alpha\beta} = 2\sum_{n\neq 0}\omega_{n0}\frac{\mathrm{Re}[\langle 0|\mu_\alpha|n\rangle\langle n|\mu_\beta|0\rangle]}{{\omega_{n0}}^2-\omega^2} \quad (2)$$

$$G'_{\alpha\beta} = -2\sum_{n\neq 0}\omega\frac{\mathrm{Im}[\langle 0|\mu_\alpha|n\rangle\langle n|m_\beta|0\rangle]}{{\omega_{n0}}^2-\omega^2} \quad (3)$$

$$A_{\alpha\beta\gamma} = 2\sum_{n\neq 0}\omega_{n0}\frac{\mathrm{Re}[\langle 0|\mu_\alpha|n\rangle\langle n|\Theta_{\beta\gamma}|0\rangle]}{{\omega_{n0}}^2-\omega^2} \quad (4)$$

The above equations describe the electric dipole−electric dipole (α), electric dipole−magnetic dipole (G), and electric dipole−electric quadrupole (A) polarizabilities. In these equations, ω denotes the frequency of the incident, ω_{n0} is the energy between the ground (0) and excited states (n), and μ, m, and Θ are the electric dipole, magnetic dipole, and electric quadrupole operators. The theoretical spectra in Figure 4b,d were obtained by adding the orientationally averaged G'^2 spectrum to the best-matched dipolar spectra in Figure 1a,c, respectively. The agreement between the experimental and theoretical spectra is evident. For instance, the experimentally

https://doi.org/10.1021/jacs.2c10132
J. Am. Chem. Soc. 2022, 144, 20561−20565

observed 1405 and 1490 cm^{-1} modes that can be assigned to in-plane aromatic CH stretching motions are not Raman active, and they can only be recovered by considering the contributions from the terms expressed by eqs 3 and 4. Indeed, we also observed spectra that can only be reconciled by considering the A^2 term, as shown in Figure S1 of the Supporting Information. This is expected, since the G' and A terms are of the same order in the expansion of molecular polarizability. In conventional implementations of Raman spectroscopy and microscopy, truncation at the dipolar term in the expansion of molecular polarizability is proper, since the wavelength of light (100s of nm) is much larger than the typical molecular length scales. The higher order terms become important when large optical field gradients (spatiotemporal) are operative. Early theoretical analyses of surface-enhanced Raman scattering spectra suggested that field gradients that vary over typical molecular length scales are needed to observe multipolar scattering efficiencies that rival normal (dipolar) Raman scattering.[19] Namely, the ratio of field-to-field gradients has to be ∼1 Å for the gradient terms to be comparable to the non-resonant Raman terms. Beyond inference through the observation of multipolar TER scattering, this requirement is easily satisfied, given the nanoscale and atomic scale[20] field localizations that have been observed in the TER geometry.[6]

At this juncture, it is important to stress that our analysis is not intended to and does not completely preclude the possibility of plasmon-induced chemistry in the TER geometry. Rather, our goal is to emphasize that multipolar Raman scattering driven by local optical field gradients needs to be taken into account in the analysis of TER spectral images. Subtle spectral changes and the appearance of modes that do not belong to the subset of Raman active modes of a molecule cannot and should not be casually assigned to plasmon-induced chemical changes, as is common practice in the surface- and tip-enhanced Raman literature. Finally, it is equally important to emphasize that our analysis does not take into consideration the possibility of resonance (e.g., with a molecule to metal charge transfer state) and only deals with static polarizabilities. Indeed, our underlying premise is that our measurements are strictly non-resonant. In addition to multipolar scattering, (transient) resonances of pure molecular or mixed molecule-metal character and vibronic effects[3] could also lead to significantly modified TER spectra. These effects should be considered in the case of resonant TER spectral imaging.

In conclusion, we carefully analyzed the TER spectral signatures of MPY molecules on gold. We found that the brightest spectra can only be understood by considering the generalized polarizabilities of the molecule. The spectral patterns that we observe and assign can be easily mistaken for the onset of chemical transformations. Studies aimed at inducing/following the latter in the TER geometry have steadily increased in number in the past few years. As such, the analysis presented herein needs to be carefully considered in the analysis of TER spectral images, particularly under ambient laboratory conditions. Beyond a handful of well-characterized model plasmon-enhanced chemical reactions, the burden of proof is high in the quest to induce/track chemical changes using TER spectral imaging.

■ ASSOCIATED CONTENT

Supporting Information

The Supporting Information is available free of charge at https://pubs.acs.org/doi/10.1021/jacs.2c10132.

Selected single-pixel spectra and their theoretical analysis, tip-engaged vs tip-retracted spectra, orientationally averaged dipolar and multipolar spectra, and experimental details (PDF)

■ AUTHOR INFORMATION

Corresponding Author

Patrick Z. El-Khoury − *Physical Sciences Division, Pacific Northwest National Laboratory, Richland, Washington 99352, United States;* orcid.org/0000-0002-6032-9006; Email: patrick.elkhoury@pnnl.gov

Authors

Alexander B. C. Mantilla − *Department of Physics and Astronomy, Washington State University, Pullman, Washington 99164, United States;* orcid.org/0000-0002-9262-1351

Chih-Feng Wang − *Physical Sciences Division, Pacific Northwest National Laboratory, Richland, Washington 99352, United States;* orcid.org/0000-0002-3085-6614

Yi Gu − *Department of Physics and Astronomy, Washington State University, Pullman, Washington 99164, United States*

Zachary D. Schultz − *Department of Chemistry and Biochemistry, The Ohio State University, Columbus, Ohio 43210, United States;* orcid.org/0000-0003-1741-8801

Complete contact information is available at: https://pubs.acs.org/10.1021/jacs.2c10132

Notes

The authors declare the following competing financial interest(s): Y.G. has equity interest in Klar Scientific.

■ ACKNOWLEDGMENTS

A.B.C.M. and Y.G. acknowledge support from the National Science Foundation (DMR-2004655). C.-F.W. was supported by the United States Department of Energy, Office of Science, Office of Biological and Environmental Research, through the bioimaging technology development program. Z.D.S. acknowledges support from the National Institutes of Health award R01 GM109988. P.Z.E. acknowledges support from the United States Department of Energy, Office of Science, Office of Basic Energy Sciences, Division of Chemical Sciences, Geosciences & Biosciences.

■ REFERENCES

(1) Langer, J.; De Aberasturi, D. J.; Aizpurua, J.; Alvarez-Puebla, R. A.; Auguie, B.; Baumberg, J. J.; Bazan, G. C.; Bell, S. E. J.; Boisen, A.; Brolo, A. G.; et al. Present and Future of Surface-Enhanced Raman Scattering. *ACS Nano* **2020**, *14*, 28−117.

(2) El-Khoury, P. Z.; Schultz, Z. D. From SERS to TERS and Beyond: Molecules as Probes of Nanoscopic Optical Fields. *J. Phys. Chem. C* **2020**, *124*, 27267−27275.

(3) Lombardi, J. R.; Birke, R. L. The Theory of Surface-Enhanced Raman Scattering. *J. Chem. Phys.* **2012**, *136*, 144704.

(4) El-Khoury, P. Z.; Hu, D. H.; Apkarian, V. A.; Hess, W. P. Raman Scattering at Plasmonic Junctions Shorted by Conductive Molecular Bridges. *Nano Lett.* **2013**, *13*, 1858−1861.

(5) Bhattarai, A.; Joly, A. G.; Hess, W. P.; El-Khoury, P. Z. Visualizing Electric Fields at Au(111) Step Edges via Tip-Enhanced Raman Scattering. *Nano Lett.* **2017**, *17*, 7131−7137.
(6) Bhattarai, A.; Crampton, K. T.; Joly, A. G.; Wang, C. F.; Schultz, Z. D.; El-Khoury, P. Z. A Closer Look at Corrugated Au Tips. *J. Phys. Chem. Lett.* **2020**, *11*, 1915−1920.
(7) Li, Z. D.; Kurouski, D. Plasmon-Driven Chemistry on Mono- and Bimetallic Nanostructures. *Acc. Chem. Res.* **2021**, *54*, 2477−2487.
(8) Bhattarai, A.; El-Khoury, P. Z. Nanoscale Chemical Reaction Imaging at the Solid-Liquid Interface via TERS. *J. Phys. Chem. Lett.* **2019**, *10*, 2817−2822.
(9) El-Khoury, P. Z.; Hess, W. P. Vibronic Raman Scattering at the Quantum Limit of Plasmons. *Nano Lett.* **2014**, *14*, 4114−4118.
(10) Wang, C. F.; Cheng, Z. H.; O'Callahan, B. T.; Crampton, K. T.; Jones, M. R.; El-Khoury, P. Z. Tip-Enhanced Multipolar Raman Scattering. *J. Phys. Chem. Lett.* **2020**, *11*, 2464−2469.
(11) O'Callahan, B. T.; El-Khoury, P. Z. A Closer Look at Tip-Enhanced Raman Chemical Reaction Nanoimages. *J. Phys. Chem. Lett.* **2022**, *13*, 3886−3889.
(12) Lee, J. H.; Tallarida, N.; Chen, X.; Liu, P. C.; Jensen, L.; Apkarian, V. A. Tip-Enhanced Raman Spectromicroscopy of Co(II)-Tetraphenylporphyrin on Au(111): Toward the Chemists' Microscope. *ACS Nano* **2017**, *11*, 11466−11474.
(13) Zoltowski, C. M.; Shoup, D. N.; Schultz, Z. D. Investigation of SERS Frequency Fluctuations Relevant to Sensing and Catalysis. *J. Phys. Chem. C* **2022**, *126*, 14547−14557.
(14) Wang, C. F.; O'Callahan, B. T.; Krayev, A.; El-Khoury, P. Z. Nanoindentation-Enhanced Tip-Enhanced Raman Spectroscopy. *J. Chem. Phys.* **2021**, *154*, 241101.
(15) O'Callahan, B. T.; Bhattarai, A.; Schultz, Z. D.; El-Khoury, P. Z. Power-Dependent Dual Analyte Tip-Enhanced Raman Spectral Imaging. *J. Phys. Chem. C* **2020**, *124*, 15454−15459.
(16) Cai, Z. F.; Kaser, T.; Kumar, N.; Zenobi, R. Visualizing On-Surface Decomposition Chemistry at the Nanoscale Using Tip-Enhanced Raman Spectroscopy. *J. Phys. Chem. Lett.* **2022**, *13*, 4864−4870.
(17) Singh, P.; Deckert, V. Local Protonation Control using Plasmonic Activation. *Chem. Commun.* **2014**, *50*, 11204−11207.
(18) Ruud, K.; Helgaker, T.; Bour, P. Gauge-Origin Independent Density-Functional Theory Calculations of Vibrational Raman Optical Activity. *J. Phys. Chem. A* **2002**, *106*, 7448−7455.
(19) Aikens, C. M.; Madison, L. R.; Schatz, G. C. The Effect of Field Gradient on SERS. *Nat. Photonics* **2013**, *7*, 508−510.
(20) Lee, J.; Crampton, K. T.; Tallarida, N.; Apkarian, V. A. Visualizing Vibrational Normal Modes of a Single Molecule with Atomically Confined Light. *Nature* **2019**, *568*, 78−82.

https://doi.org/10.1021/jacs.2c10132
J. Am. Chem. Soc. 2022, 144, 20561−20565